

ISSN Online: 1947-3826 ISSN Print: 1949-2421

# Measurement and Modeling of LoRa Signal in Multi-Floor Home Environment

# **Chen Zhong**

Department of Economics and Information Management, Shanghai University of Finance and Economics Zhejiang College, Iinhua China

Email: chen.zhong.jku@gmail.com

How to cite this paper: Zhong, C. (2025) Measurement and Modeling of LoRa Signal in Multi-Floor Home Environment. *Communications and Network*, **17**, 1-19. https://doi.org/10.4236/cn.2025.171001

Received: February 8, 2025 Accepted: February 25, 2025 Published: February 28, 2025

Copyright © 2025 by author(s) and Scientific Research Publishing Inc. This work is licensed under the Creative Commons Attribution International License (CC BY 4.0).

http://creativecommons.org/licenses/by/4.0/





## **Abstract**

The Internet of Things (IoT) is rapidly developing with the promotion of new technologies such as LoRa, which offers extensive coverage, low power consumption, and strong anti-interference capabilities. This study focuses on the application of LoRa technology in multi-floor home environments, particularly addressing the challenges of signal multipath propagation. We conducted comprehensive measurements of LoRa signal strength and path loss across different floors and rooms. Through our path loss model analysis, notable differences were observed in Line-of-Sight (LOS) and Non-Line-of-Sight (NLOS) environments, with initial path loss values of 58.32 decibels and 51.52 decibels, respectively, and standard deviations of 18.42 decibels for LOS and 2.84 decibels for NLOS. Temporal fading analysis, using Rayleigh and Rician distributions, revealed significant variations in signal strength between daytime and nighttime, with some rooms being more stable during the daytime and others more stable at nighttime due to differences in the architectural structure and functionality of various rooms within the home environment. Packet reception rate (PRR) ranged from 89.07% to 99.89%, highlighting the reliability of data transmission under different conditions. This research fills a critical gap in the literature by providing empirical data on indoor multi-floor home environments and significantly contributes by verifying and modeling path loss and temporal fading, thereby improving the design and deployment strategies for LoRa-based smart home systems.

## **Keywords**

LoRa, Smart Home, Path Loss Mode, Rician, Rayleigh, Packet Reception Rate

#### 1. Introduction

The rapid advancement of the IoT [1] has significantly impacted various sectors,

such as smart building and smart home applications [2]-[4]. These indoor multifloor environments present unique challenges due to signal multipath propagation [5] caused by various obstacles. In the realm of smart homes, various wireless communication technologies are employed, including Wi-Fi [6], Zigbee [7] and Bluetooth [8]. Wi-Fi, while widely used for high-bandwidth applications such as video streaming and internet browsing, suffers from high power consumption and limited range, making it less ideal for battery-powered IoT devices. Zigbee, although being low-power and suitable for short-range communication, faces issues with scalability and interference from other devices operating in the same frequency bands. Bluetooth, commonly used for personal area networks, has limitations in range and the number of devices it can effectively manage. These limitations highlight the need for a more robust solution like LoRa [9], which can provide reliable communication over longer distances with lower power consumption due to its extensive coverage and robustness against interference. It is a modulation technique for low-power wide-area networks (LPWANs) [10] and stands out in the context of smart homes for its ability to offer reliable, long-range communication with minimal power requirements. It supports various applications, including environmental monitoring, energy management, security systems, and automation of household appliances. The extensive coverage of LoRa ensures connectivity even in large multi-floor buildings, overcoming the range limitations of other wireless technologies. However, the current research area lacks a comprehensive study of path loss [11], large-scale fading (LSF) [12], multipath effects, and temporal fading [13] of the LoRa signal in a multi-floor home environment. Understanding these factors is crucial for optimizing the deployment and performance of LoRa-based smart home systems. This study aims to address the existing gaps in the literature by conducting an in-depth investigation into the behavior of LoRa signals in multi-floor home environments. The primary objectives include measuring and modeling path loss, analyzing the multipath propagation effect, understanding the temporal fading of LoRa signals, and measuring and analyzing PRR. The contributions of this study are as follows:

- This study conducted comprehensive measurements of LoRa signal strength in a multi-floor home environment.
- This study modeled a path loss model for indoor multi-floor home environments and calculated and analyzed the parameters and applicability of three models.
- This study analyzed temporal fading under the multipath propagation effect using Rayleigh and Rician distributions.

The remainder of this paper is organized as follows: Section 0 introduces related work, and Section 0 illustrates the path loss model. The measurement method is presented in Section 1. The experiments and their results are presented in Section 3. Finally, section 5 concludes the paper.

## 2. Related Work

In wireless transmission networks, the wireless signal is inevitably subject to path

loss due to various obstacles like walls, trees, and air that hinder its propagation. [14]-[21] explored the use and validation of path loss models in different application scenarios, including Low Power Wide Area Networks (LPWAN), millimeterwave wireless networks, indoor ultra-wideband propagation, dense small cell networks, device-to-device communication, and hospital environments. The studies employed various path loss models, such as the Free Space Path Loss (FSPL) model, regression coefficient models, the Longley-Rice Irregular Terrain Model (ITM), and the Log-Distance model. These models' accuracy and applicability were verified through experimental measurements and simulations. Results indicated significant differences in model performance across different environments, and incorporating terrain data or environment-specific parameters can enhance path loss prediction accuracy [19] [21]. However, the models were complex, with many parameters and high computational demands, making real-time applications challenging [19]; they were highly environment-dependent, showing varying performance in different settings, lacking universality [20]; they had large prediction errors, with some models showing significant errors in actual signal prediction [14] [21]; there was a lack of comprehensive evaluation, with most studies missing multi-environment and multi-scenario validation [15] [18]; and there were application limitations, with some models only applicable to specific frequency bands and scenarios, restricting their wider adoption and use [16] [19] [20].

Large-scale fading is an important factor to consider during long-distance wire-less transmission. [22]-[26] discussed the application of LSF in various scenarios, including non-Bayesian activity detection, large-scale MIMO systems, disaster relief scenarios, uplink capacity analysis, and sparse activity detection in multi-cell large-scale MIMO. These studies proposed using LSF information to improve detection performance, enhance system capacity, build communication models for disaster scenarios, and increase spectrum efficiency. However, these studies commonly had the drawback of making many ideal condition assumptions, overlooking the complexity and variability of real-world environments, which limits the accuracy and robustness of the models and methods in practical applications.

During long-distance wireless transmission, there are usually various obstacles, so the shadow fading effect cannot be ignored. [27]-[31] primarily investigated shadow fading models and their effects in different environments and applications. [27] explored the correlation of shadow fading between links in multi-hop wireless networks, proposing a statistical model and validating its impact on network connectivity. [28] proposed a method for detecting co-moving wireless devices using shadow fading by correlating signal strength variations. [29] compared two shadow fading models in ultra-wideband and other wireless systems, highlighting the advantages of the Gamma distribution model in performance analysis. [30] introduced a statistical method based on log moments to estimate the composite fast fading and shadowing distribution in wireless communication. [31] presented a new fading-shadowing model and analyzed its performance in emergency wireless communications with unmanned aerial vehicles equipped with reconfigurable

intelligent surfaces. However, these models were complex and challenging to implement directly in practical applications; some models made many assumptions specific to certain environments, lacking generality, and some methods required extensive experimental data for validation, increasing application difficulty and cost.

In order to better study the signal attenuation during LoRa long-range wireless transmission, LoRa transmission modeling is needed. [32]-[38] employed various models to describe path loss in different environments, including the FSPL, Log-Normal Shadowing Model (LNSM), Okumura-Hata model, and machine learning techniques such as Random Forest and Recurrent Neural Network (RNN). These studies aimed to optimize LoRa network coverage and performance by accurately modeling path loss to enhance the reliability and efficiency of IoT applications. These models performed differently across environments: traditional models like FSPL [32] [33] [38] were accurate in obstacle-free environments but had large errors in complex settings; LNSM [34] and Okumura-Hata [35] models considered environmental impacts through empirical data but may still produce errors in new application scenarios. Machine learning methods, like Random Forest [35] and RNN [32], significantly improved path loss prediction accuracy but faced challenges in adaptability to new environments. Overall, the accuracy and applicability of LoRa path loss models required further optimization to suit the variable realworld application environments.

# 3. Modeling Methodology

### 3.1. Large-Scale Fading

LSF, also known as path loss, is a key component in the characterization of radio wave propagation in wireless communication systems. It describes the attenuation of the received signal strength (RSS) over long distances and various obstacles, such as buildings and terrain, between the transmitter (Tx) and receiver (Rx). This type of fading primarily results from the combined effects of path loss and shadowing. In LSF analysis, it is crucial to model the path loss accurately, analyze the shadowing effect, and determine the relevant distances in different environments.

#### 3.1.1. Path Loss Model

Path loss refers to the reduction in power density of an electromagnetic wave as it propagates through space. It is influenced by the distance between the Tx and Rx and the environment through which the wave travels. It is typically modeled using the following equation [39].

$$PL(d) = PL(d_0) + 10n\log\frac{d}{d_0} + X_{\sigma}$$
 (1)

where:

- *d* is the separation distance between Tx and Rx.
- $X_{\sigma}$  is a zero-mean Gaussian distributed variable with standard deviation  $\sigma$  .

•  $PL(d_0)$  is the path loss at the reference distance (1 meter in this study). The least squares regression [40] was used to calculate  $PL(d_0)$ . First, for each measurement sample i, the error  $e_i$  is defined as follows:

$$e_i = PL_i - \left(PL(d_0) + 10n\log(d_i)\right) \tag{2}$$

where  $PL_i$  is the measured path loss at distance  $d_i$ . The sum of the squared errors S can be computed as follows:

$$S = \sum_{i=1}^{N} e_i^2 = \sum_{i=1}^{N} \left[ PL_i - \left( PL(d_0) + 10n \log(d_i) \right) \right]^2$$
 (3)

where N is the total number of measurement samples. To calculate  $PL(d_0)$ , the partial derivative of the objective function of  $PL(d_0)$ , and let the derivative be zero:

$$\frac{\partial S}{\partial PL(d_0)} = -2\sum_{i=1}^{N} \left[ PL_i - \left( PL(d_0) + 10n\log(d_i) \right) \right] = 0 \tag{4}$$

From Equation (4), the  $PL(d_0)$  can be solved as follows:

$$PL(d_0) = \frac{1}{N} \left( \sum_{i=1}^{N} PL_i - 10n \sum_{i=1}^{N} \log d_i \right)$$
 (5)

• *n* is the path loss exponent, which varies by environment. For example, in free space, *n* is typically 2, while in urban or indoor environments, *n* can range from 2 to 4 or higher. The same least-squares regression is used to calculate *n*, which is derived as follows:

$$n = \frac{\sum_{i=1}^{N} PL_i \log d_i - PL(d_0) \sum_{i=1}^{N} \log d_i}{10 \sum_{i=1}^{N} (\log d_i)^2}$$
(6)

## 3.1.2. Shadowing Effect

Shadowing [41], or log-normal fading [42], refers to the variations in signal strength caused by obstacles like buildings, trees, and other large objects obstructing the LOS between Tx and Rx. The term  $X_{\sigma}$  in the path loss model accounts for these random variations. It is modeled as a zero-mean Gaussian random variable with standard deviation  $\sigma$ , which is derived as follows:

$$\sigma = \sqrt{\frac{1}{N} \sum_{i=1}^{n} \left( X_i - \overline{X} \right)} \tag{7}$$

where  $X_i$  is the deviation between the *i*-th measured sample and the predicted values.  $\overline{X}$  is the mean of all deviations.

## 3.1.3. Decorrelation Distance

Decorrelation distance [43] is a key parameter in characterizing the spatial correlation of shadow fading in wireless communication environments. It is defined as the distance over which the autocorrelation of the signal's shadow fading component drops to a specified threshold: 0.1 in this study. This distance indicates how quickly the signal variations due to shadowing become uncorrelated as the receiver

moves away from the transmitter. The normalized autocorrelation function  $R_{xx}(i)$ , is given by:

$$R_{xx}(i) = \frac{\sum_{p=1}^{N-i} X_p X_{p+i}}{\sum_{q=1}^{N} X_q^2}$$
 (8)

where  $X_p$ ,  $X_{p+i}$  and  $X_q$  are the deviation of the shadow fading measurement samples at different locations.

## 3.2. Temporal Fading

In wireless communication, temporal fading is caused by multipath propagation and the Doppler effect. However, since devices in smart homes are typically stationary, the Doppler effect is more relevant to mobile devices, making temporal fading in smart homes primarily influenced by multipath propagation alone. Multipath effects refer to signals traveling from the transmitter to the receiver along multiple paths, including direct, reflected, diffracted, and scattered paths. The signals arriving at the receiver at different times cause their superposition to result in either constructive interference (signal enhancement) or destructive interference (signal attenuation), leading to fluctuations in the RSS. Scattering refers to the phenomenon where wireless signals encounter obstacles that are irregular or smaller than the signal wavelength (such as leaves or rough surfaces of buildings), causing the signals to scatter in various directions and resulting in a more dispersed energy distribution at the receiver, which receives multipath signals from different directions. Temporal fading is the change in signal strength over time caused by these phenomena. Temporal fading can be divided into slow fading and fast fading: slow fading is caused by large-scale changes (such as the macroscopic movement of devices or building obstructions), resulting in relatively gradual changes in signal strength; fast fading is caused by small-scale changes (such as multipath propagation and phase interference), leading to rapid changes in signal strength. By analyzing the measured RSS with Rayleigh [44] and Rician [45] distributions, we can gain a more comprehensive understanding of the impact of temporal fading on LoRa signals.

#### 3.2.1. Rayleigh Distribution

In a multipath propagation environment without a LOS, the RSS follows the Rayleigh distribution. The Rayleigh distribution is applicable to scenarios where all signals are from scattered paths, with its probability density function (PDF) [46] given by:

$$f(r) = \frac{r}{\sigma^2} e^{-\frac{r^2}{2\sigma^2}}, (r \ge 0)$$
(9)

where r is the RSS, and  $\sigma$  is the standard deviation of the signal strength. The cumulative distribution function (CDF) [47] of the Rayleigh distribution is:

$$F(r) = 1 - e^{-\frac{r^2}{2\sigma^2}}, (r \ge 0)$$
 (10)

#### 3.2.2. Rician Distribution

The Rician distribution model is used to describe the RSS in environments with LOS and multipath propagation. Its PDF is given by:

$$f(r) = \frac{r}{\sigma^2} e^{-\frac{r^2 + A^2}{2\sigma^2}} I_0\left(\frac{rA}{\sigma^2}\right), (r \ge 0)$$
(11)

where r is the RSS, A is the amplitude of the direct path signal,  $\sigma$  is the standard deviation of the multipath components, and  $I_0$  is the modified Bessel function of the first kind. Among the parameters of Rician distribution, the Rician factor K has important physical significance and represents the ratio between the power of the direct-view path signal and the power of the multipath-scattered signal, which reflects the relative strengths of the direct-view path and multipath effects in the channel [48]. This factor is defined as follows:

$$K = \frac{A^2}{2\sigma^2} \tag{12}$$

When K is high, the direct path signal dominates, resulting in smaller signal fluctuations and fading, which is suitable for outdoor open environments or LOS transmission scenarios. While K is low, the scattered path signals dominate, leading to larger signal fluctuations and fading, commonly found in indoor environments or scenarios with many obstacles. When K=0, the Rician distribution degenerates into the Rayleigh distribution, where all signals are from scattered paths.

## 3.3. Coverage Estimation

We estimated the coverage range of the LoRa signal in an indoor multi-floor home environment. The selected parameters are listed in **Table 1**. We assume an ambient attenuation coefficient of 45, an attenuation coefficient of 15 dB per floor, a signal-to-noise ratio (SNR) of –6 dB, a transmitter and receiver antenna gain of 0 dBi for both, and 0 dB connector loss. By estimating using the Free Space Path Loss Model [49] and the ITU-R P.1238 model [50], the coverage range of the LoRa signals is derived: 137.37 meters. This distance allows a single gateway to completely cover the entire three-layer measurement environment.

**Table 1.** LoRa physical layer settings.

Spreading factor	Bandwidth (KHz)	Coding rate		Frequence (MHz)	Transmit Power (dBm)	
	500	4/5	8	470 - 510	20	

#### 4. Measurement Method

On the third floor, we set the LOS and NLOS measurements as illustrated in Figure 1, with the gateway on the desk in the study. In the LOS scenario, a total of 80 points were measured, all aligned linearly with the gateway. The first point was positioned 0.1 meters from the gateway, with each subsequent point spaced 0.1

meters apart. In the NLOS scenario, a total of 31 points were measured and aligned linearly. The first point was placed in the adjacent bathroom, with a horizontal distance d1 of 1.7 meters and a vertical distance d2 of 0.3 meters from the gateway. Each subsequent point was measured at intervals of 0.1 meters. The distance d from the gateway to each of the 31 points is calculated using the Pythagorean theorem [51].

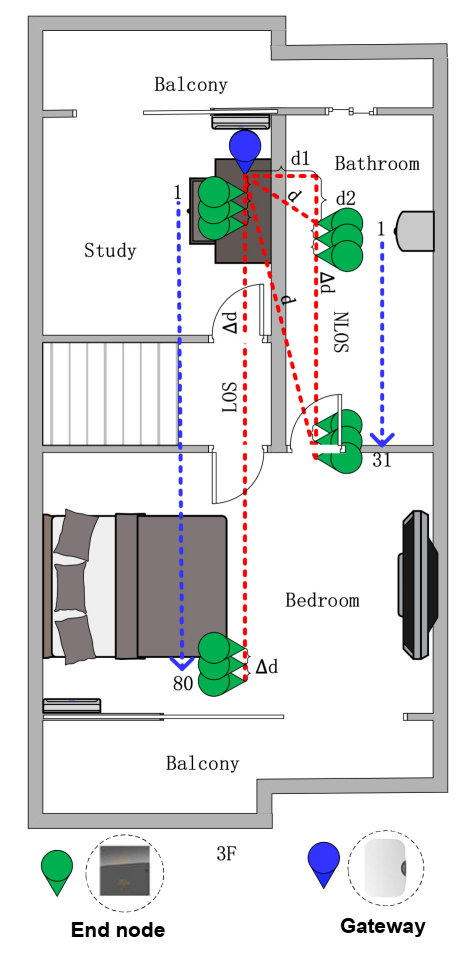


Figure 1. LOS and NLOS measurement mode.

The layout schematic in Figure 2 illustrates the distribution of gateways and end nodes throughout the home. Appliances and furniture are installed on the first floor: an air conditioner, gas stove, water heater, tables, chairs and sofa, refrigerator, television, and microwave oven. The second floor features two beds, a water heater, three air conditioners, and a bathroom. The third floor is equipped with two air conditioners, a television, a bed, a water heater, and a sofa. The measuring environment is characterized by a complex array of household furniture and appliances. Figures 3(a)-(c) show the placement of measurement locations for some of the end nodes contained: the first-floor living room, the third-floor bathroom, and the third-floor study. The gateway was placed in the third-floor study, as depicted in Figure 3(d), also highlighted by a red circle. The antennas of the

gateway and the end nodes were oriented vertically and horizontally relative to the ground, respectively. The measurement environment consisted of rooms with brick walls and wooden furniture.

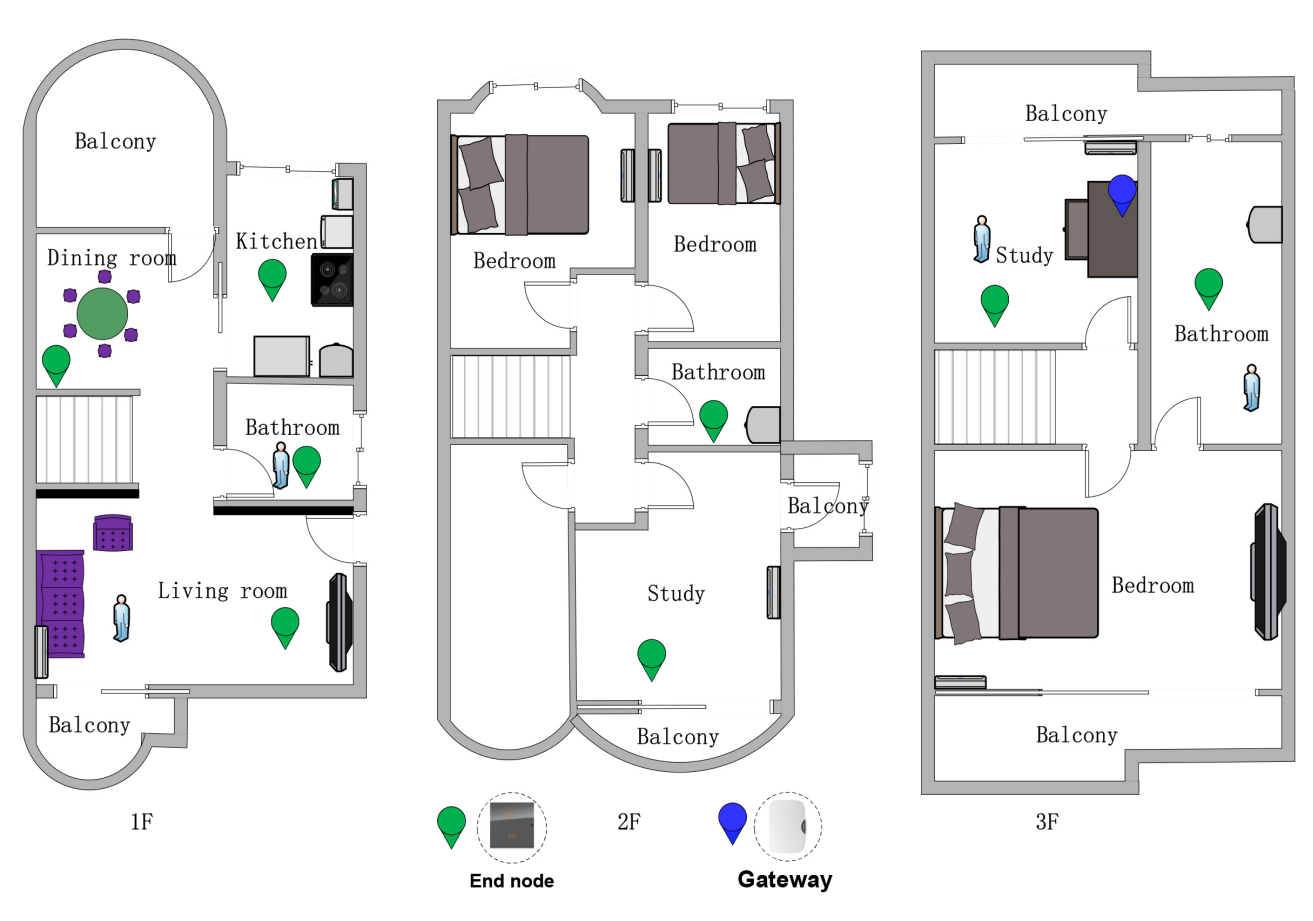


Figure 2. 3-story home building measurement point locations.



Figure 3. Measurement of physical photos.

# 5. Results

# 5.1. Large Scale Fading

Compare the path loss fitting performance of the non-fixed model, fixed model, and free-space model (FSM). Figure 4(a) and Figure 4(b) show the fitting results of the three models, where blue dots represent measurement samples, the red solid lines represent the non-fixed model, the orange dashed lines represent the fixed

model, and the gray dashed lines represent the FSM. **Table 2** shows the results for both scenarios. We found that the fixed model performs well at short distances but shows significant deviations at longer distances due to its failure to fully account for the nonlinear effects of distance on path loss. The FSM assumes no obstacles in the propagation path and ignores multipath effects and terrain variations. In contrast, the non-fixed model has flexible parameters that better adapt to various factors in the actual wireless propagation environment, such as building obstacles, terrain variations, and multipath effects.

Table 2. Results of the LOS and NLOS.

LSF Scenario	Non-Fixed Intercept (computed from the Equation (5))			Fixed Intercept (measured at $d_0$ )		
	PL(d <sub>0</sub> ) [dB]	n [-]	σ [dB]	PL(d <sub>0</sub> ) [dB]	n [-]	σ [dB]
LOS	58.32	2.34	18.42	51.52	48.47	2.84
NLOS	57.00	2.26	18.50	67.00	6.00	5.25
Average	57.66	2.3	18.46	59.26	27.23	4.04
FSM	59.95	-	-	40.05	-	-

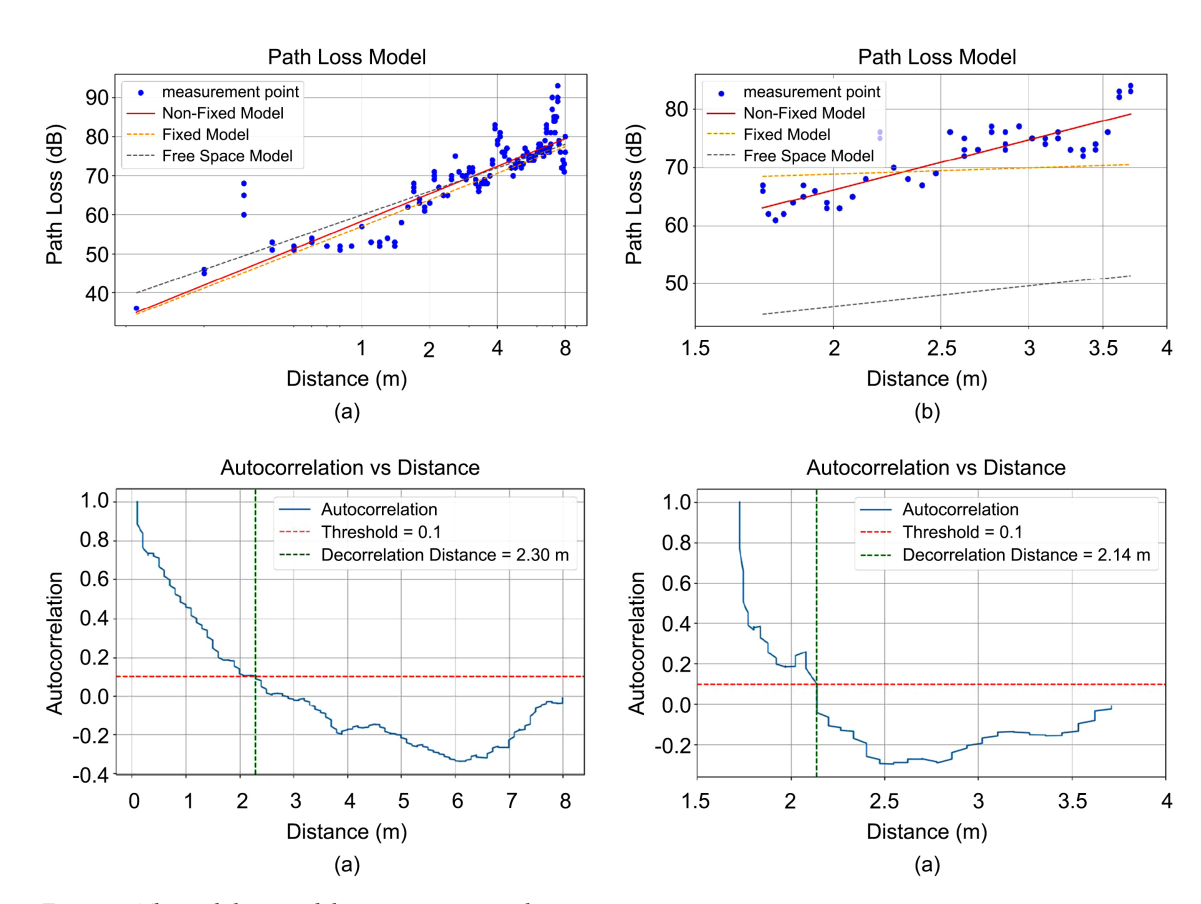


Figure 4. The path loss model measurement result.

Figure 4(c) and Figure 4(d) show the decorrelation distance of LOS and NLOS with values of 2.3 m and 2.14 m, respectively. The shorter decorrelation distance in NLOS environments compared to LOS is primarily due to the increased reflections, scattering, and diffraction in NLOS propagation paths. These factors cause more frequent and severe fluctuations in signal strength, leading to a faster decrease in autocorrelation.

# 5.2. Temporal Fading

The RSS samples collected from various rooms in a multi-floor building demonstrate significant variations in signal strength between daytime (7 - 22) and nighttime (22 - 7). The RSS samples for the first-floor rooms, including the bathroom, dining room, kitchen, and living room, exhibit similar patterns of variation. Figures 5(a)-(d) all illustrate that during the daytime, the signal strength tends to be weaker and more variable. This instability is due to increased activity levels within the house, leading to more physical obstructions and higher interference from other electronic devices in use. Conversely, during the nighttime, the signal strength is observed to be more stable and generally stronger. The reduced human activity and lesser usage of electronic devices during the nighttime contribute to a clearer signal path with fewer interferences and obstructions. The second-floor rooms, comprising the bathroom and study, exhibit similar trends in their RSS samples, as shown in Figure 5(e) and Figure **5(f)**. For the third-floor rooms, including the bathroom and study, the RSS samples, depicted in Figure 5(g) and Figure 5(h), follow the same pattern observed on the lower floors. This pattern indicates the significant impact of environmental factors on LoRa signal performance.

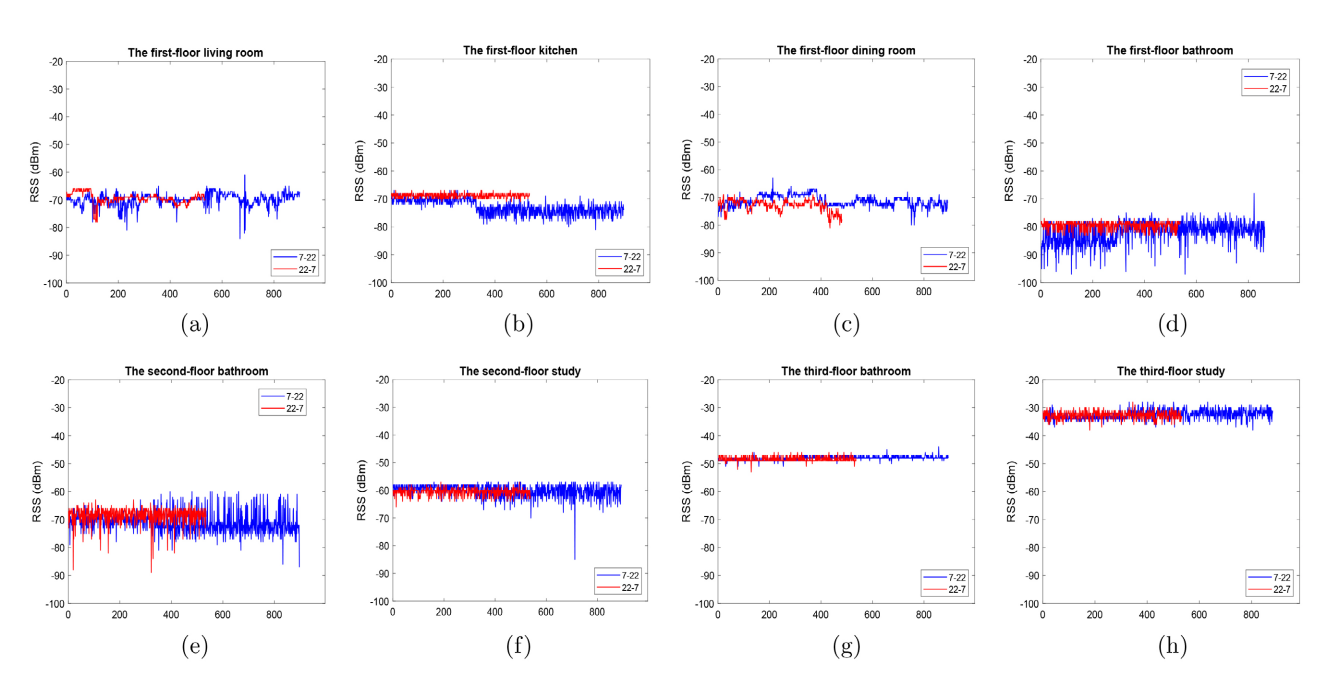


Figure 5. RSS values of the end nodes deployed on the 8th floor and 9th floor at 2 pm - 7 pm and 7 pm - 12 pm, respectively.

**Figure 6** shows the PDF and CDF of the RSS samples for the first floor. We can see that the *K* values of all measured end nodes are higher during the daytime than at nighttime. It is expected that *K* values might be higher during the nighttime due to more stable environments. However, in this analysis, higher *K* values during the daytime are observed in several rooms. This can be attributed to specific usage patterns and structural factors: The living room, kitchen, and dining room are used throughout the daytime for various activities, which involve intermittent rather than continuous use of electronic devices. These rooms benefit from natural light and ventilation during the daytime, reducing the reliance on electronic lighting and appliances that generate interference. The controlled and less intensive use of electronic devices in these rooms during the daytime leads to a more stable environment for signal propagation, resulting in higher *K* values.

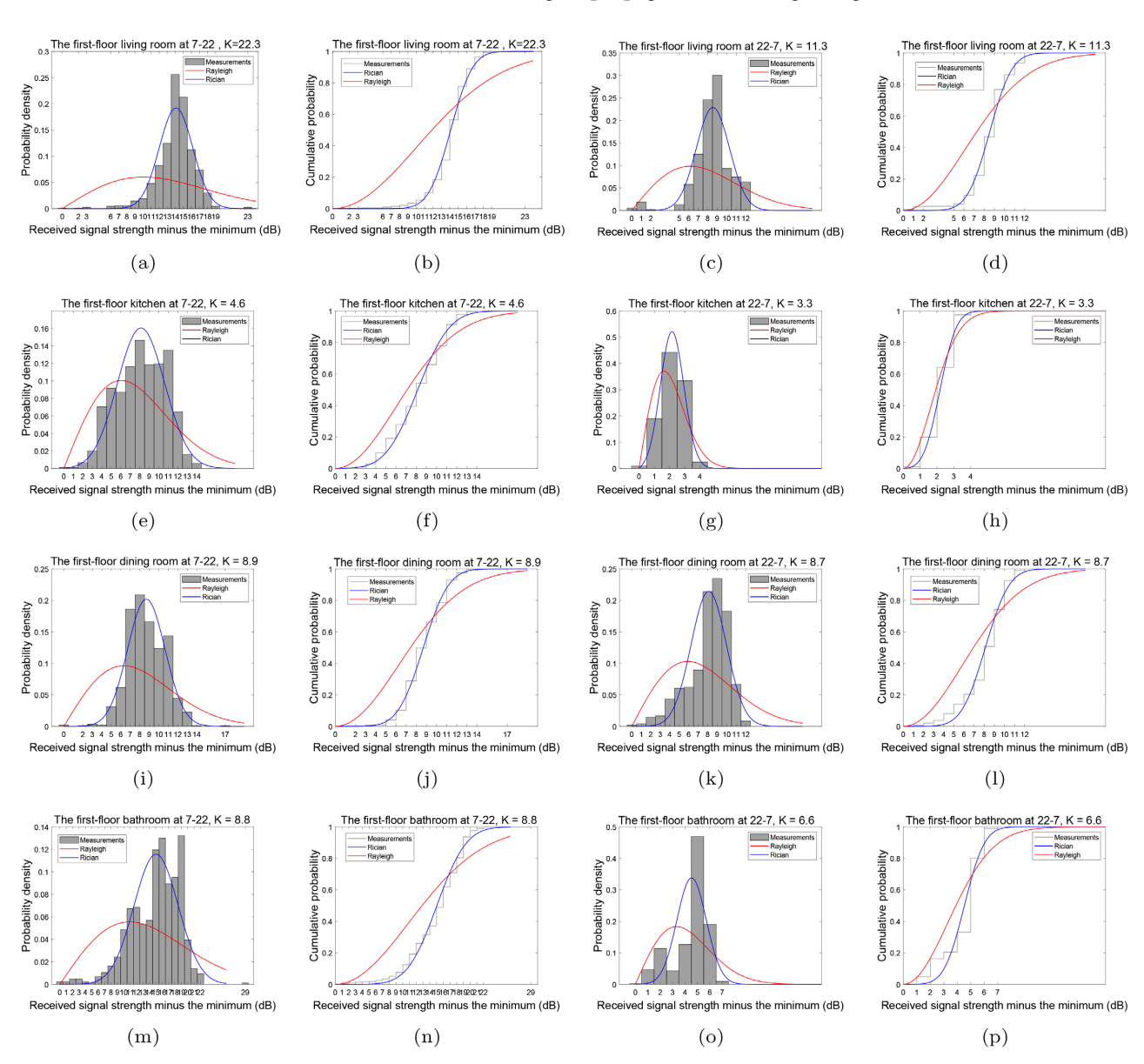


Figure 6. PDF and CDF of the end nodes deployed on the 1st floor at 7 am - 10 pm and 10 pm - 7 am, respectively.

The measurement results of the second floor are shown in Figure 7. During the daytime, the bathroom exhibits a lower K value compared to the nighttime. This substantial difference can be attributed to increased human activity and the use of reflective surfaces such as mirrors and tiles during the daytime, which enhance multipath effects. During the nighttime, reduced activity and fewer interactions with these surfaces result in a higher K value due to a more stable environment with fewer multipath reflections. In contrast, the study room demonstrates a different pattern. The daytime K value is higher than the nighttime K value. The higher K values during the daytime can be explained by its specific usage characteristics. During the daytime, this room is used for focused tasks such as studying or remote work, involving a stable setup with minimal movement and fewer active electronic devices compared to other times. This consistent environment reduces multipath reflections and signal fluctuations, leading to higher K values. At night, the study may be repurposed for other activities or left unused, which could introduce variability in the environment and lower the Kvalue due to different patterns of electronic device usage and human activity.

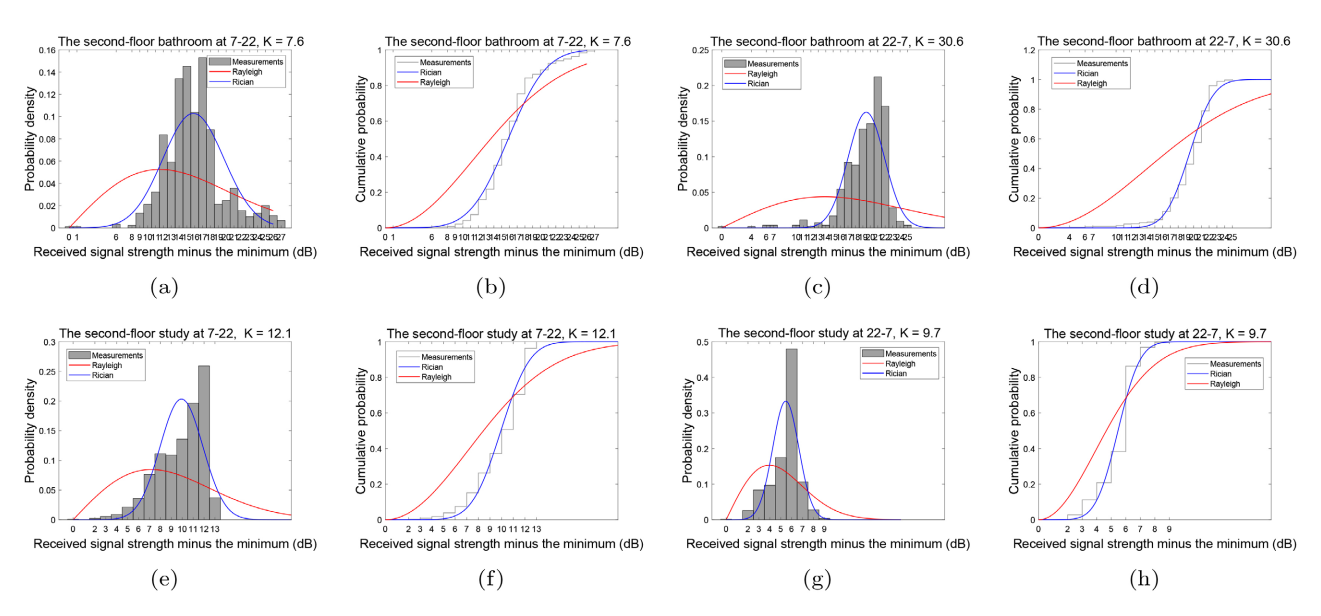


Figure 7. PDF and CDF of the end nodes deployed on the 2nd floor at 7 am - 10 pm and 10 pm - 7 am, respectively.

**Figure 8** illustrates the PDF and CDF of the RSS samples for the third floor. Analysis of the *K* values for the third floor showed a consistent trend of lower *K* values during the daytime than the nighttime for both the bathroom and the study. In the bathroom, frequent usage of water fixtures and mirrors during the daytime introduces more multipath effects, causing a greater dispersion of signal paths and thereby reducing the *K* factor. Similarly, the study room is likely to experience increased activity during the daytime, such as studying, working, and the use of electronic devices, which contribute to a higher number of signal reflections and a lower *K* value. In contrast, during the nighttime, human activity decreases significantly, resulting in fewer interactions with reflective surfaces and electronic

devices. This reduction in activity leads to a more stable environment with fewer multipath reflections, thereby increasing the *K* factor.

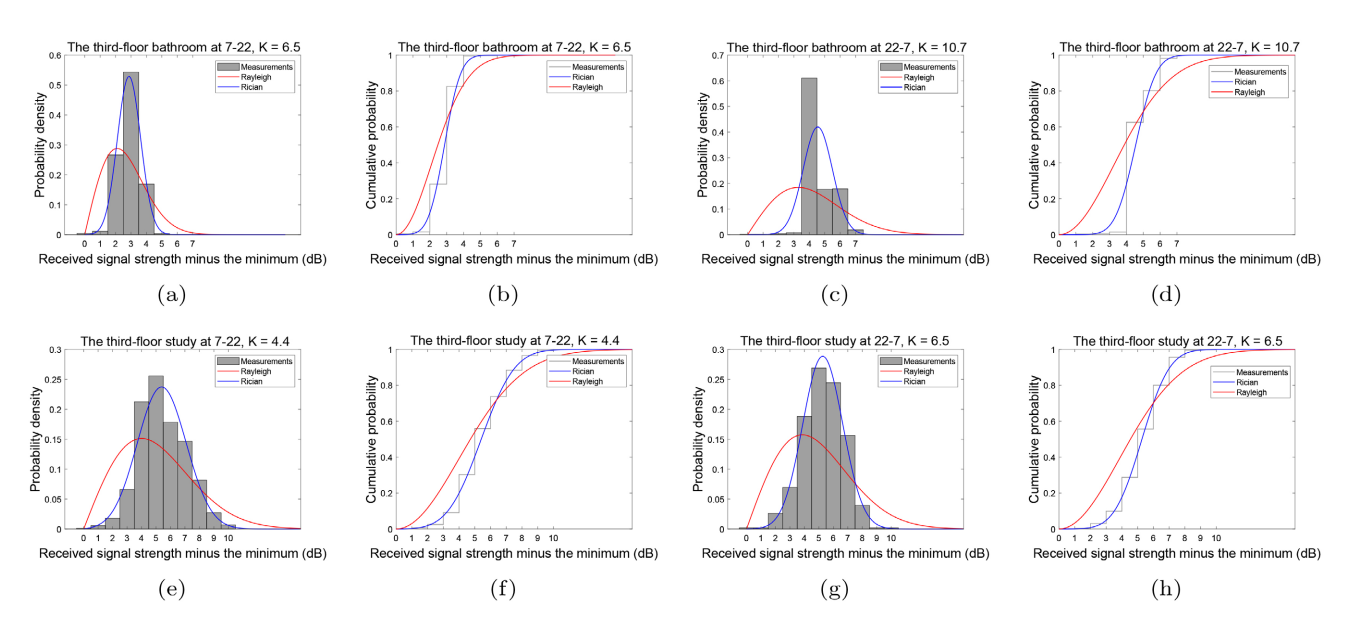
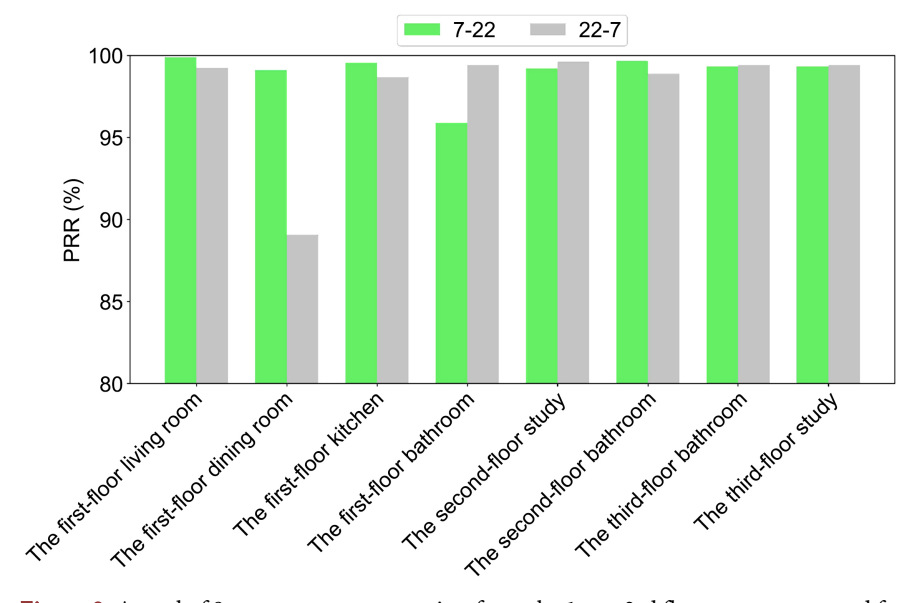


Figure 8. PDF and CDF of the end nodes deployed on the 3rd floor at 7 am - 10 pm and 10 pm - 7 am, respectively.

## 5.3. Coverage



**Figure 9.** A total of 8 room measurement sites from the 1st to 3rd floors were measured for reception success during daytime and nighttime.

**Figure 9** illustrates the PRR at various measurement locations during the two time periods. Overall, the PRR during the daytime are slightly higher than those during the nighttime, and we found that certain rooms have higher PRR during the daytime, such as the first-floor living room (99.89%), the first-floor kitchen (99.56%), the second-floor bathroom (99.67%), and the third-floor study (99.33%).

The primary reasons for the higher PRR during the daytime in these rooms are related to the specific patterns of activity and the nature of interference sources. During the daytime, many electronic devices that cause interference (such as televisions and entertainment systems) are used more heavily in the evening, reducing their impact during the daytime. Additionally, during the daytime, doors and windows are more likely to be open, allowing for better air circulation and less obstruction to signal propagation. Conversely, the rooms with higher PRR during the nighttime include the first-floor dining room (89.07%), the first-floor bathroom (99.44%), the second-floor study (99.22%), and the third-floor bathroom (99.44%). The reasons for higher PRR during the nighttime in these rooms are due to reduced external interference and environmental noise, as well as decreased human activity, which reduces signal blockage and reflection, thereby improving PRR. Particularly, the third-floor study, where the gateway is placed, shows consistently high PRR both daytime and nighttime due to its central role in signal reception, experiencing the least interference and having the shortest signal propagation path.

#### 6. Conclusion

Based on the findings and analysis presented in this paper, we conducted a comprehensive investigation into the behavior of LoRa signals in multi-floor home environments, focusing on path loss, multipath propagation, temporal fading, and PRR. The measurements revealed significant differences in signal strength and path loss across different floors and rooms, highlighting the challenges of signal multipath propagation in complex indoor environments. The study modeled a non-fixed path loss model, which demonstrated higher accuracy and adaptability compared to the fixed model and FSM. Temporal attenuation analysis shows that there is a significant difference in signal strength between daytime and nighttime, with some rooms having higher signal stability during the daytime and others during the nighttime due to the different functions and usage of each room. Additionally, our evaluation of the PRR indicated high reliability in data transmission across different conditions. The results underscore the importance of understanding indoor signal propagation to optimize the deployment and performance of LoRa-based smart home systems. Future research will explore machine learning for real-time signal prediction and the interactions between LoRa and other IoT technologies to further enhance the robustness and efficiency of smart home systems, advancing the field of indoor wireless communications and expanding the use of LoRa technology in the growing IoT space.

## **Conflicts of Interest**

The author declares no conflicts of interest regarding the publication of this paper.

## References

[1] You, I., Pau, G., Salerno, V.M. and Sharma, V. (2019) Special Issue 'Internet of Things

- for Smart Homes'. Sensors, 19, Article 4173. https://doi.org/10.3390/s19194173
- [2] Opipah, S., Qodim, H., Miharja, D., Hamidi, E.A.Z. and Juhana, T. (2020) Prototype Design of Smart Home System Base on LoRa. 2020 6th International Conference on Wireless and Telematics (ICWT), Yogyakarta, 3-4 September 2020, 1-5. https://doi.org/10.1109/ICWT50448.2020.9243643
- [3] Zhong, C. and Nie, X. (2024) A Novel Single-Channel Edge Computing LoRa Gateway for Real-Time Confirmed Messaging. *Scientific Reports*, 14, Article No. 8369. <a href="https://doi.org/10.1038/s41598-024-59058-8">https://doi.org/10.1038/s41598-024-59058-8</a>
- [4] Zhong, C., Nie, X.Z. and Peng, P. (2024) Novel Power Conservation Methods for LoRa-Based Infrared Sensors in Smart Building. *IEEE Sensors Journal*, **24**, 15311-15326.
- [5] Kamann, A., Held, P., Perras, F., Zaumseil, P., Brandmeier, T. and Schwarz, U. (2018) Automotive Radar Multipath Propagation in Uncertain Environments. 2018 21st International Conference on Intelligent Transportation Systems (ITSC), Maui, HI, USA, 4-7 November 2018, 859-864. https://doi.org/10.1109/ITSC.2018.8570016
- [6] Tozlu, S. (2011) Feasibility of Wi-Fi Enabled Sensors for Internet of Things. 2011 7th International Wireless Communications and Mobile Computing Conference, Istanbul, 4-8 July 2011, 291-296. https://doi.org/10.1109/IWCMC.2011.5982548
- [7] Ramya, C.M., Shanmugaraj, M. and Prabakaran, R. (2011) Study on Zig-Bee Technology. 2011 3rd International Conference on Electronics Computer Technology, Kanyakumari, 8-10 April 2011, 297-301. https://doi.org/10.1109/ICECTECH.2011.5942102
- [8] Danbatta, S.J. and Varol, A. (2019) Comparison of Zigbee, Z-Wave, Wi-Fi, and Bluetooth Wireless Technologies Used in Home Automation. 2019 7th International Symposium on Digital Forensics and Security (ISDFS), Barcelos, 10-12 June 2019, 1-5. https://doi.org/10.1109/ISDFS.2019.8757472
- [9] Pham, C. and Ehsan, M. (2021) Dense Deployment of LoRa Networks: Expectations and Limits of Channel Activity Detection and Capture Effect for Radio Channel Access. Sensors, 21, Article 825. <a href="https://doi.org/10.3390/s21030825">https://doi.org/10.3390/s21030825</a>
- [10] Shea, S. (2017) LPWAN (Low-Power Wide Area Network).

  <a href="https://www.techtarget.com/iotagenda/definition/LPWAN-low-power-wide-area-network">https://www.techtarget.com/iotagenda/definition/LPWAN-low-power-wide-area-network</a>
- [11] Durgin, G., Rappaport, T. and Xu, H. (1998) Measurements and Models for Radio Path Loss and Penetration Loss in and around Homes and Trees at 5.85 GHz. *IEEE Transactions on Communications*, **46**, 1484-1496. https://doi.org/10.1109/26.729393
- [12] Rashdan, I., De Ponte Muller, F., Jost, T., Sand, S. and Caire, G. (2019) Large-Scale Fading Characteristics and Models for Vehicle-to-Pedestrian Channel at 5-GHz. IEEE Access, 7, 107648-107658. https://doi.org/10.1109/ACCESS.2019.2933264
- [13] Tang, P., Zhang, J., Molisch, A., Smith, P., Shafi, M. and Tian, L. (2018) Estimation of the K-Factor for Temporal Fading from Single-Snapshot Wideband Measurements. *IEEE Transactions on Vehicular Technology*, 68, 49-63. <a href="https://doi.org/10.1109/TVT.2018.2878352">https://doi.org/10.1109/TVT.2018.2878352</a>
- [14] Tang, W., Chen, M., Chen, X., Dai, J., Han, Y., Di Renzo, M., Zeng, Y., Jin, S., Cheng, Q. and Cui, T. (2020) Wireless Communications with Reconfigurable Intelligent Surface: Path Loss Modeling and Experimental Measurement. *IEEE Transactions on Wireless Communications*, 20, 421-439. https://doi.org/10.1109/TWC.2020.3024887
- [15] Sulyman, A., Alwarafy, A., Maccartney, G., Rappaport, T. and Alsanie, A. (2016) Directional Radio Propagation Path Loss Models for Millimeterwave Wireless Networks in the 28-, 60-, and 73-GHz Bands. *IEEE Transactions on Wireless Communications*,

- 15, 6939-6947. https://doi.org/10.1109/TWC.2016.2594067
- [16] Muqaibel, A., Safaai-Jazi, A., Attiya, A., Woerner, B. and Riad, S. (2006) Path-Loss and Time Dispersion Parameters for Indoor UWB Propagation. *IEEE Transactions on Wireless Communications*, 5, 550-559. https://doi.org/10.1109/TWC.2006.1611085
- [17] Ding, T., Ding, M., Mao, G., Lin, Z. and Lopez-Perez, D. (2015) Uplink Performance Analysis of Dense Cellular Networks with LoS and NLoS Transmissions. *IEEE Transactions on Wireless Communications*, 15, 2365-2380. https://doi.org/10.1109/TWC.2015.2503391
- [18] Santos, P.M., Abrudan, T. and Aguiar, A. (2014) Impact of Position Errors on Path loss Model Estimation for Device-to-Device Channels. *IEEE Transactions on Wireless Communications*, 13, 2353-2361. https://doi.org/10.1109/TWC.2014.040214.131082
- [19] Kyro, M., Haneda, K., Simola, J., Nakai, K., Takizawa, K., Hagiwara, H. and Vaini-kainen, P. (2011) Measurement Based Path Loss and Delay Spread Modeling in Hospital Environments at 60 GHz. *IEEE Transactions on Wireless Communications*, 10, 2423-2427. https://doi.org/10.1109/TWC.2011.062211.101601
- [20] Ding, T., Ding, M., Mao, G., Lin, Z. and Lopez-Perez, D. (2017) Uplink Performance Analysis of Dense Cellular Networks with LoS and NLoS Transmissions. *IEEE Transactions on Wireless Communications*, 16, 2601-2613. https://doi.org/10.1109/TWC.2017.2669023
- [21] Linka, H., Rademacher, M. and Aliu, O. (2018) Path Loss Models for Low-Power Wide-Area Networks: Experimental Results Using LoRa. *VDE ITG-Fachbericht Mobilkommunikation*, Osnabrück, 16 May 2018, 1-33.
- [22] Yang, A., He, Z., Xing, C., Fei, Z. and Kuang, J. (2015) The Role of Largescale Fading in Uplink Massive Mimo Systems. *IEEE Transactions on Vehicular Technology*, 65, 477-483. <a href="https://doi.org/10.1109/TVT.2015.2397553">https://doi.org/10.1109/TVT.2015.2397553</a>
- [23] Van Chien, T., Mollen, C. and Bjornson, E. (2018) Large-Scale-Fading Decoding in Cellular Massive Mimo Systems with Spatially Correlated Channels. *IEEE Transactions on Communications*, 67, 2746-2762. https://doi.org/10.1109/TCOMM.2018.2889090
- [24] Chen, Z., Sohrabi, F. and Yu, W. (2021) Sparse Activity Detection in Multicell Massive Mimo Exploiting Channel Large-Scale Fading. *IEEE Transactions on Signal Processing*, 69, 3768-3781. <a href="https://doi.org/10.1109/TSP.2021.3090679">https://doi.org/10.1109/TSP.2021.3090679</a>
- [25] Fengler, A., Haghighatshoar, S., Jung, P. and Caire, G. (2021) Non-Bayesian Activity Detection, Large-Scale Fading Coefficient Estimation, and Unsourced Random Access with a Massive Mimo Receiver. *IEEE Transactions on Information Theory*, 67, 2925-2951. <a href="https://doi.org/10.1109/TIT.2021.3065291">https://doi.org/10.1109/TIT.2021.3065291</a>
- [26] Chen, L., Loschonsky, M. and Reindl, L. (2010) Large-Scale Fading Model for Mobile Communications in Disaster and Salvage Scenarios. 2010 *International Conference* on Wireless Communications & Signal Processing (WCSP), Suzhou, 21-23 October 2010, 1-5. https://doi.org/10.1109/WCSP.2010.5633059
- [27] Agrawal, P. and Patwari, N. (2009) Correlated Link Shadow Fading in Multihop Wireless Networks. *IEEE Transactions on Wireless Communications*, 8, 4024-4036. https://doi.org/10.1109/TWC.2009.071293
- [28] Chandrasekaran, G., Ergin, M., Gruteser, M., Martin, R., Yang, J. and Chen, Y. (2009) Decode: Exploiting Shadow Fading to Detect Comoving Wireless Devices. *IEEE Transactions on Mobile Computing*, 8, 1663-1675. <a href="https://doi.org/10.1109/TMC.2009.131">https://doi.org/10.1109/TMC.2009.131</a>

- [29] Abdi, A. and Kaveh, M. (2011) A Comparative Study of Two Shadow Fading Models in Ultrawideband and Other Wireless Systems. *IEEE Transactions on Wireless Com*munications, 10, 1428-1434. <a href="https://doi.org/10.1109/TWC.2011.031611.100309">https://doi.org/10.1109/TWC.2011.031611.100309</a>
- [30] Reig, J. and Rubio, L. (2013) Estimation of the Composite Fast Fading and Shadowing Distribution Using the Log-Moments in Wireless Communications. *IEEE Transac*tions on Wireless Communications, 12, 3672-3681. <a href="https://doi.org/10.1109/TWC.2013.050713.120054">https://doi.org/10.1109/TWC.2013.050713.120054</a>
- [31] Chen, Y., Cheng, W. and Zhang, W. (2023) Reconfigurable Intelligent Surface Equipped UAV in Emergency Wireless Communications: A New Fading-Shadowing Model and Performance Analysis. *IEEE Transactions on Communications*, **72**, 1821-1834. <a href="https://doi.org/10.1109/TCOMM.2023.3336223">https://doi.org/10.1109/TCOMM.2023.3336223</a>
- [32] Liu, L., Yao, Y., Cao, Z. and Zhang, M. (2021) DeepLoRa: Learning Accurate Path Loss Model for Long Distance Links in LPWAN. *IEEE INFOCOM* 2021—*IEEE Conference* on Computer Communications, Vancouver, 10-13 May 2021, 1-10. https://doi.org/10.1109/INFOCOM42981.2021.9488784
- [33] Rademacher, M., Linka, H., Horstmann, T. and Henze, M. (2021) Path Loss in Urban Lora Networks: A Large-Scale Measurement Study. 2021 *IEEE* 94th *Vehicular Technology Conference* (*VTC*2021-*Fall*), Norman, 27-30 September 2021, 1-6. <a href="https://doi.org/10.1109/VTC2021-Fall52928.2021.9625531">https://doi.org/10.1109/VTC2021-Fall52928.2021.9625531</a>
- [34] Budi, B. (2024) Distance Testing on Point to Point Communication with Lora Based on Rssi and Log Normal Shadowing Model. *Journal of Energy and Electrical Engineering*, **5**, 89-93.
- [35] Masadan, N., Habaebi, M. and Yusoff, S. (2018) LoRa LPWAN Propagation Channel Modelling in IIUM Campus. 2018 7th International Conference on Computer and Communication Engineering (ICCCE), Kuala Lumpur, 19-20 September 2018, 14-19. https://doi.org/10.1109/ICCCE.2018.8539327
- [36] Anzum, R., Habaebi, M., Islam, M., Hakim, G., Khandaker, M., Osman, H., Alamri, S. and Abdelrahim, E. (2022) A Multiwall Path-Loss Prediction Model Using 433 MHz LoRa-WAN Frequency to Characterize Foliage's Influence in a Malaysian Palm Oil Plantation Environment. Sensors, 22, Article 5397. <a href="https://doi.org/10.3390/s22145397">https://doi.org/10.3390/s22145397</a>
- [37] González-Palacio, M., Tobón-Vallejo, D., Sepúlveda-Cano, L.M., Rúa, S., Pau, G. and Le, L.B. (2022) LoRaWAN Path Loss Measurements in an Urban Scenario Including Environmental Effects. *Data*, **8**, Article 4. <a href="https://doi.org/10.3390/data8010004">https://doi.org/10.3390/data8010004</a>
- [38] Geng, Z. and Deng, H. (2022) Wireless Signal Propagation Path Loss Estimation. 2014 *IEEE Antennas and Propagation Society International Symposium* (*APSURSI*), Memphis, 6-11 July 2014, 953-954.
- [39] Kurt, S. and Tavli, B. (2017) Path-Loss Modeling for Wireless Sensor Networks: A Review of Models and Comparative Evaluations. *IEEE Antennas and Propagation Magazine*, 59, 18-37. <a href="https://doi.org/10.1109/MAP.2016.2630035">https://doi.org/10.1109/MAP.2016.2630035</a>
- [40] Watson, G. (1967) Linear Least Squares Regression. *The Annals of Mathematical Statistics*, **38**, 1679-1699. <a href="https://doi.org/10.1214/aoms/1177698603">https://doi.org/10.1214/aoms/1177698603</a>
- [41] Lee, J. and Baccelli, F. (2018) On the Effect of Shadowing Correlation on Wireless Network Performance. *IEEE INFOCOM* 2018—*IEEE Conference on Computer Communications*, Honolulu, 16-19 April 2018, 1601-1609. <a href="https://doi.org/10.1109/INFOCOM.2018.8485965">https://doi.org/10.1109/INFOCOM.2018.8485965</a>
- [42] Alouini, M.-S. and Simon, M. (2002) Dual Diversity over Correlated Lognormal Fading Channels. *IEEE Transactions on Communications*, **50**, 1946-1959. https://doi.org/10.1109/TCOMM.2002.806552

- [43] Xu, W., Kim, J., Huang, W., Kanhere, S., Jha, S. and Hu, W. (2019) Measurement, Characterization, and Modeling of Lora Technology in Multifloor Buildings. *IEEE Internet of Things Journal*, 7, 298-310. <a href="https://doi.org/10.1109/JIOT.2019.2946900">https://doi.org/10.1109/JIOT.2019.2946900</a>
- [44] Al-Noor, N.H. and Assi, N.K. (2020) Rayleigh-Rayleigh Distribution: Properties and Applications. *Journal of Physics: Conference Series*, 1591, Article 012038. <a href="https://doi.org/10.1088/1742-6596/1591/1/012038">https://doi.org/10.1088/1742-6596/1591/1/012038</a>
- [45] Karakuş, O., Kuruoglu, E. and Achim, A. (2021) A Modification of Rician Distribution for SAR Image Modelling. https://doi.org/10.20944/preprints202010.0209.v1
- [46] Ren, M., Zhang, Q. and Zhang, J. (2019) An Introductory Survey of Probability Density Function Control. Systems Science & Control Engineering, 7, 158-170. https://doi.org/10.1080/21642583.2019.1588804
- [47] Minh, H., Lavane, K., Lanh, L., Thinh, L., Cong, N., Ty, T., Downes, N. and Kumar, P. (2022) Developing Intensity-Duration-Frequency (IDF) Curves Based on Rainfall Cumulative Distribution Frequency (CDF) for Can Tho City, Vietnam. *Earth*, 3, 866-880. <a href="https://doi.org/10.3390/earth3030050">https://doi.org/10.3390/earth3030050</a>
- [48] Abdi, A., Tepedelenlioglu, C., Kaveh, M. and Giannakis, G. (2001) On the Estimation of the K Parameter for the Rice Fading Distribution. *IEEE Communications Letters*, 5, 92-94. <a href="https://doi.org/10.1109/4234.913150">https://doi.org/10.1109/4234.913150</a>
- [49] Katircioğlu, O., Isel, H., Ceylan, O., Taraktas, F. and Yagci, H.B. (2011) Comparing Ray Tracing, Free Space Path Loss and Logarithmic Distance Path Loss Models in Success of Indoor Localization with RSSI. 2011 19th Telecommunications Forum (TEL-FOR) Proceedings of Papers, Belgrade, 22-24 November 2011, 313-316. https://doi.org/10.1109/TELFOR.2011.6143552
- [50] Batalha, I.S., Castro, B.S.L., Lopes, A.V.R., Pelaes, E.G. and Cavalcante, G.P.S. (2015) Cross-Layer Modeling for Video Quality Loss on WLANs. 2015 9th European Conference on Antennas and Propagation (EuCAP), Lisbon, 13-17 April 2015, 1-5.
- [51] Agarwal, R. (2020) Pythagorean Triples before and after Pythagoras. *Computation*,8, Article 62. <a href="https://doi.org/10.3390/computation8030062">https://doi.org/10.3390/computation8030062</a>